Environmental Science and Ecotechnology 31 (2026) 100698

Contents lists available at ScienceDirect

Environmental Science and Ecotechnology

journal homepage: www.journals.elsevier.com/environmental-science-and-ecotechnology/

Original Research

Positive bacteria–phage interactions drive sulfamethoxazole removal

Ying Liu [a,1], Xiaomeng Wei [b,1], Maozhen Han [c,1], Boyu Li [d], Shaoyong Lu [e], Haiming Wu [f], Xiaohui Liu [d,*], Fengchang Wu [e]

[a] School of Environment and Geography, Shandong Key Laboratory of Synergistic Control of Complex Multi-Media Pollution, Qingdao University, Qingdao, 266071, China
[b] College of Resources and Environment, Northwest Agriculture and Forestry University, Yangling, 712100, China
[c] School of Life Sciences, Anhui Medical University, Hefei, 230032, China
[d] Key Laboratory of Marine Environment and Ecology, Ministry of Education and College of Environmental Science and Engineering, Ocean University of China, Qingdao, 266100, China
[e] State Key Laboratory of Environmental Criteria and Risk Assessment, Chinese Research Academy of Environmental Sciences, Beijing, 100012, China
[f] School of Environmental Science & Engineering, Shandong University, Qingdao, 266237, China

ARTICLE INFO

Article history:
Received 30 April 2025
Received in revised form
4 April 2026
Accepted 4 April 2026

Keywords:
Wetland sediments
Viruses
Auxiliary metabolic genes
Sulfamethoxazole
Antibiotic resistance genes

ABSTRACT

Antibiotics such as sulfonamides are ubiquitous environmental contaminants that pose severe ecological risks globally. Constructed wetlands are critical systems for mitigating these pollutants, where diverse microbial communities drive complex biogeochemical transformations. Within these ecosystems, bacteriophages are the most abundant biological entities, capable of shaping bacterial community structure and function through lytic infection and gene transfer. Virus-encoded auxiliary metabolic genes (AMGs) can specifically modulate host metabolism to enhance survival under chemical stress. However, the precise role of viruses in regulating both the degradation of antibiotics and the dissemination of antibiotic resistance genes (ARGs) remains poorly understood. Here we show that positive bacteria-phage interactions significantly improve sulfamethoxazole (SMX) removal while concurrently restricting the transfer of ARGs. Using sediment microcosm experiments, we demonstrate that the addition of phage-concentrated solutions increases SMX removal efficiency by up to 35%. Viruses achieve this by enriching specific SMX-degrading bacteria and augmenting bacterial metabolic capacity through the expression of AMGs related to energy production and extracellular polymeric substance synthesis. Furthermore, lytic viruses act as biological blockers, significantly reducing the total relative abundance of ARGs by directly lysing antibiotic-resistant host cells rather than promoting transduction. Our findings highlight the profound ecological influence of viruses in shaping microbial responses to pollutant stress. Regulating these viral communities presents a promising biological strategy to enhance the bioremediation of emerging contaminants and mitigate the global health risks of antibiotic resistance.

1. Introduction

Viruses are noncellular microorganisms that cannot perform metabolic functions autonomously and must parasitize host cells to survive and reproduce. Phages, viruses that infect bacterial cells, are the most abundant biological entities on earth and help shape the composition of microbial communities via lytic infection [1]. In addition, extensive and complex gene transfer between viruses and their hosts can affect the function and stress tolerance of a microbial community [2]. Specifically, virus-encoded auxiliary metabolic genes (AMGs) have been shown to shape bacterial metabolism and influence local and global biogeochemical processes, such as nutrient and toxic pollutant transformations [3,4]. Previous studies have shown that phage-encoded AMGs related to microbial antioxidant and pollutant degradation improve bacterial growth under benzo[a]pyrene [4] or pesticide stress [5]. These phenomena indicate that viruses can affect pollutant removal efficiency, the dissemination of resistance genes, and microbial

* Corresponding author.
E-mail address: lxh7786@ouc.edu.cn (X. Liu).
[1] Ying Liu, Xiaomeng Wei, and Maozhen Han contributed equally to this work.

https://doi.org/10.1016/j.ese.2026.100698

adaptation to chemical contamination. However, our knowledge of the interactions that occur between viruses and bacteria under these stresses remains limited.

Sulfonamides (SAs) are widely used in the prevention and treatment of human and animal diseases. However, the processes implemented in sewage treatment plants to remove SAs are ineffective, and they are present at high concentrations in surface water, sediment, and soil [6]. For example, the highest concentrations of sulfamethoxazole (SMX) have been detected in lakes and rivers, where it poses the greatest ecological risk [7,8]. SMX residues are also environmental stressors for microorganisms in natural and sewage treatment systems, such as wetlands. In turn, microbial polymers significantly influence the solid–liquid distribution, degradation, and transformation of SMX [9]. The types of microorganisms involved are diverse, including bacteria and viruses. Most research has focused on the response of a single microbial population to antibiotic stress [10–12]. Significantly, exposure of viruses carrying genes associated with SA degradation to SA could result in the positive selection of AMGs that degrade SA, potentially shifting the composition of a microbial community. Thus, understanding the adaptability and interactions among different types of microorganisms under antibiotic stress is essential to elucidating microbial community assembly mechanisms.

More importantly, viruses can promote or inhibit the dissemination of antibiotic resistance genes (ARGs) via transduction and different lytic–lysogenic strategies; hence, they can affect the spread of drug resistance and the emergence of antibiotic resistance. However, the role of viruses in ARG transfer remains unclear [13,14]. This is because conflicting evidence has been obtained across studies on different viral communities and survival strategies under varying environmental conditions [2,15]. Effects of viruses on material transformation in soil systems are influenced by environmental heterogeneity [15]. Therefore, it is vital to understand the viral population structure and function across different environments to optimize the viral contribution to antibiotic bioremediation and reduce ARG transfer [16]. Furthermore, there is a need to explore virus–host interactions under antibiotic stress and to identify the role of viruses in regulating antibiotic transformation.

In constructed wetlands designed to treat sewage, the sediment is a hotspot for SMX accumulation, migration, and transformation. Furthermore, microbial colonization and pollutant removal occur in the sediment. Hence, SMX and viruses tend to co-locate in wetland sediments. Given that viruses cannot pass through the physical barriers inserted to trap larger molecules in the sediment, viruses are abundant in the sediment and inevitably participate in complex interactions with microorganisms and pollutants in the sediment. However, the population structure and function of viruses in wetland sediments remain unclear.

To address the abovementioned knowledge gaps, we aimed to deepen our understanding of the key antibiotic-removal processes mediated by virus–bacteria interactions and provide a theoretical basis for developing viral regulation strategies to reduce antibiotic pollution. To achieve these aims, we explored viral population structure, virus–host interactions under SMX stress, and the impact of viruses on SMX transformation and bacterial resistance in sediment using tangential flow filtration (TFF) technology in combination with viromics and metagenomics.

2. Materials and methods

2.1. Experimental setup

Sediment was collected from a full-scale constructed wetland, sieved through a 2-mm filter, and divided into three samples. We sterilized the first sample at 121 °C for 30 min in a high-pressure sterilization pot. We used the second sample to extract a phage concentrated solution (PCS) and a bacterial inoculation solution (BIS) via TFF (methodology in Supplementary Text S1). The PCS extraction method was developed to optimize efficiency (Supplementary Text S2 and Fig. S1). The third sample was incubated with 1 mg L^{-1} SMX at 25 °C for 30 days.

The microcosm experiments were conducted in 250 mL glass beakers. A total of 100 g of sterile sediment was added to each beaker. We established four systems to investigate the effects of the PCS on the structure and function of the sediment microbiome under SMX stress, SMX transformation, and ARG transfer (Fig. 1). The control system included only BIS (from 100 g sediment). To identify the role of viruses, we assembled the B100V system by mixing BIS and PCS at a 1:1 ratio (prepared from 100 g sediment). The B300V system, with a 1:3 BIS-to-PCS ratio (prepared from 100 g sediment), was established to explore the influence of virus concentration. The B100DV system combined BIS with DPCS at a 1:1 ratio, where the DPCS was prepared from 100 g of sediment pre-incubated with SMX, to test how SMX exposure alters PCS effects. Three beakers were used for each experimental condition to ensure that data were available from three biological replicates. The experimental samples were incubated with synthetic domestic sewage (Supplementary Table S1) for one week (incubation period), and then SMX (100 μg L^{-1}) was added to all groups (stable operation period). All experiments were conducted using a batch sequence strategy with a hydraulic retention time of 3 days for 108 days.

2.2. Analytical methods

We detected and identified SMX and its intermediate products via high performance liquid chromatography-tandem mass spectrometry (HPLC-MS/MS, LCMS-8040, Shimadzu, Japan) and UPLC-QTOF-MS (Scientific Export, Canada) using previously described methods [17]. Organic matter, total nitrogen, and total phosphorus were measured using the potassium dichromate oxidation external heating method, the Kjeldahl method after sulfuric acid digestion, and the molybdenum antimony spectrophotometric method after NaOH alkali melting, respectively. The dissolved organic carbon concentration was measured using a total organic carbon analyzer (TOC–VCPH, Shimadzu, Japan). Extracellular polymeric substances (EPS) were extracted from sediment samples using a modified heat extraction method [18] and characterized as soluble, loosely bound, or tightly bound (Supplementary Text S3). The protein and polysaccharide components of the EPS were determined using Coomassie Brilliant Blue G-250 and phenol-sulfuric acid reagents, respectively [19].

2.3. DNA extraction and sequencing

We used the DNeasy PowerSoil DNA Isolation Kit (Qiagen, Germany) and MagPure Viral DNA/RNA Mini LQ Kit (Angen Biotech Co., China) to extract the total DNA and viral DNA from 0.5 g sediment samples, respectively, following the manufacturer's

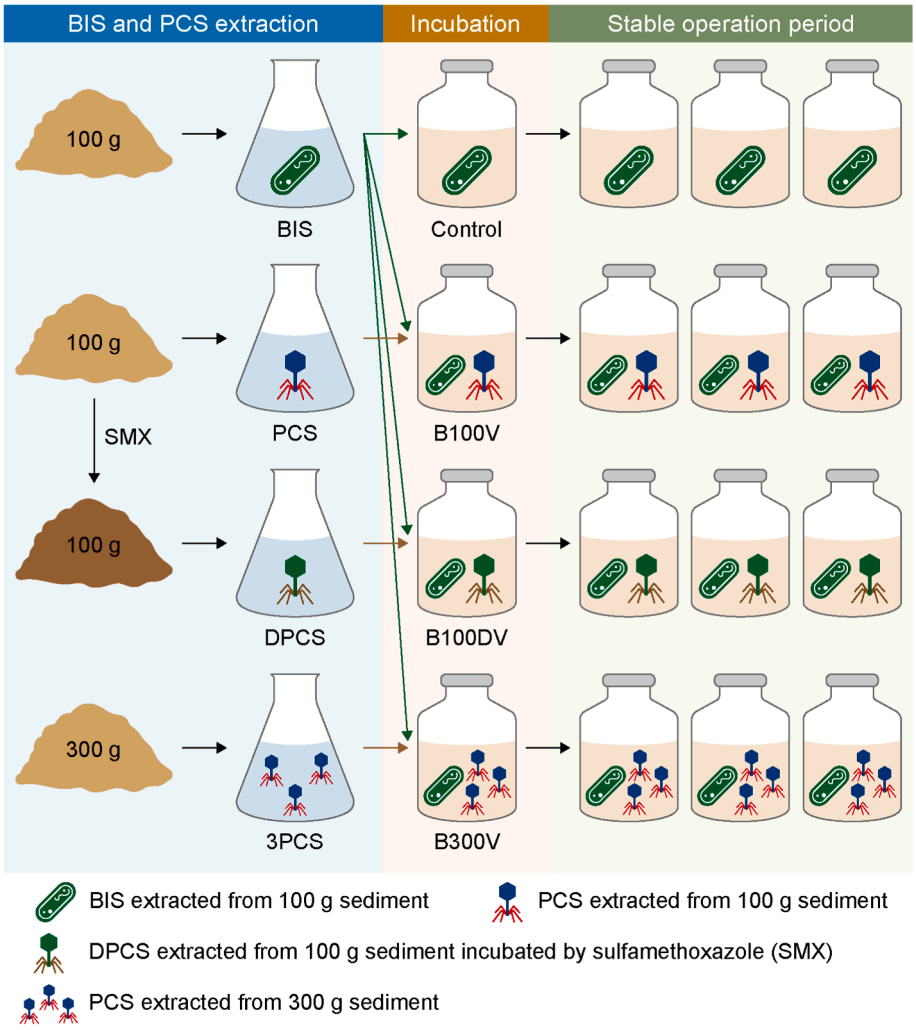

Fig. 1. Schematic illustration of the experimental design. Bacterial inoculum solution (BIS) and phage-concentrated solution (PCS) were extracted from wetland sediment and used to establish the treatment groups, followed by incubation and a stable-operation period. BIS was extracted from 100 g of sediment and added to all systems. PCS was prepared either from 100 g of sediment (PCS), 300 g of sediment (3PCS), or 100 g of sediment pre-incubated with sulfamethoxazole (SMX; DPCS). The treatment groups were Control (BIS only), B100V (BIS combined with PCS from 100 g of sediment), B300V (BIS combined with PCS from 300 g of sediment), and B100DV (BIS combined with DPCS).

instructions. The quality and integrity of the extracted total DNA was verified using 1% agarose gel. Metagenomic sequencing was conducted using the Illumina NovaSeq 6000 platform in PE150 mode (Magigene, China). Whole-genome amplification of viral DNA was performed using a REPLI-g Cell WGA & WTA Kit (Qiagen, Germany). The quality of the phage DNA-amplified products was verified using a 1% agarose gel, a Qubit 3.0 instrument, and a Nanodrop One spectrophotometer (Thermo Fisher, MA, USA) [4]. Fastp (v0.20.1; default settings) was used to obtain high-quality sequencing reads from the metagenome and metavirome datasets [20]. We determined the composition of the microbial communities using MetaPhlAn4 (https://github.com/biobakery/MetaPhlAn). Subsequently, we used MEGAHIT (v1.2.9) [21] to cross-assemble the remaining reads of each system to obtain the bacterial and viral contigs. The meta-large and meta-sensitive modes were used for the metagenome and metavirome sequencing reads, respectively. The filtered thresholds for the nonviral (including bacterial and archaeal) and viral contigs were set to 500 bp and 300 bp, respectively [21]. Open reading frames (ORFs) were predicted from nonviral contigs and viral contigs using Prodigal (v2.6.3) [22].

2.4. Bacterial taxonomic assignment, virus identification, and functional annotation

Bacterial taxonomy was assigned using Blast (v2.9.0+) and the NCBI-NR database [21]. Virsorter2 (v2.2.3) [23] was applied for virus identification, and all identified viral contigs were extracted (Supplementary Text S4). We constructed a gene-sharing network of viruses across the different samples using vConTACT 2.0 [24], which assigns viral sequences to viral clusters (VCs). We annotated the viral contig taxonomy by querying the IMG/VR database (v4) with BLASTn [24]. We then predicted the hosts of the viral contigs using CHERRY, a popular tool known for its high performance and accuracy [25]. The lysogenic and lytic viral contigs and AMGs were detected using the built-in machine-learning method in VIBRANT [26]. ARGs were annotated using blastp based on the SARG (v2.2) database (*e*-value $\leq 1 \times 10^{-5}$, similarity $\geq$80%, and query coverage $\geq$70%) [27]. We estimated gene abundances with BBmap [28], and and normalized counts as reads per kilobase million (RPKM) for each sample. For nonviral contigs, we mapped ORF functional annotations to the kyoto encyclopedia of gene and genome (KEGG) database using MEGAN [29] and DIAMOND [29], and summarized the results as heatmaps. The components of the phosphorus cycle

were filtered according to the KEGG ontology (KO) numbers reported in previous studies [28]. We used the METABOLIC [30] to annotate genes and profile components of the carbon, nitrogen, and sulfur cycles. DefenseFinder was used to identify antiviral defense systems [31].

2.5. Statistical analysis

Data analysis and visualization were primarily performed using R. The alpha-diversities (including simpson, and shannon) of the viral and bacterial compositions were calculated using the vegan package (https://github.com/vegandevs/vegan) in R (v4.0.3), and the differences were compared using the F-test. Differences among the viruses, bacterial compositions, and functional traits were assessed using PERMANOVA, and principal component analysis (PCA) was performed to visualize the differences. The venn results were visualized using the UpSetR package (https://github.com/hms-dbmi/UpSetR). The functional genes heatmap was constructed using an online platform (http://cloudtutu.com.cn/). The viral and bacterial co-occurrence networks were visualized using Gephi (v0.9.2) [32] based on Pearson correlation coefficients. The key functional metabolic pathways were identified using a random forest model (RFM) and the rfPermute package (https://github.com/cran/rfPermute). A structural equation model (SEM) was fitted using statistical product and service software automatically (SPSSAU, https://spssau.com/indexs.html) to identify the shift in the virus–bacteria relationship in response to the PCS, thereby revealing the contribution of the PCS to SMX removal. We used a multiple regression model (MRM) to explore the relationships between SMX removal and multiple factors. Before fitting the MRM, we assessed redundancy among environmental variables using the VARCLUS function in Hmisc and excluded variables with Spearman's $\rho^2 > 0.7$. We then performed stepwise variable removal by excluding nonsignificant variables ($p < 0.05$) and refitting the model using the ecodist package until all retained variables were significant.

3. Results and discussion

3.1. Impact of viruses on SMX removal and transformation

The addition of PCS improved SMX removal efficiency (Fig. 2a). Compared to the control, the B100V treatment exhibited a 35.0% higher SMX removal efficiency. Increasing PCS within a certain range was beneficial for SMX removal: B300V exhibited a 7.8% higher SMX removal efficiency than B100V. Treating sediment with B100DV was also more efficient than treating it with B100V for SMX removal. Moreover, PCS affected the physical and chemical characteristics of the sediment (Supplementary Text S5), as evidenced by an increase in organic matter content and a decrease in SMX in the B100V-treated samples (Supplementary Table S2). Interestingly, the time required to reach the highest SMX removal efficiency was not affected by PCS concentration or source. B300V and B100DV showed the same regulatory effect on SMX removal, with similar average removal efficiencies. These results indicate that SMX removal efficiency can be increased by adding PCS; however, environmental conditions should be considered (e.g., pH, temperature, and nutrient limitations) [33].

Phage-concentrated solution altered the SMX transformation. The possible degradation pathways (Fig. 2b) and intermediate products (Supplementary Table S3) are presented. The initial steps in the biodegradation of SMX generally involve the cleavage of N–C and S–N bonds. In Pathway I, the PCS, especially DPCS, accelerated the isomerization of the isoxazole ring to generate 4-amino-N-(5-methyl-3-oxazole) benzene sulfonamide. Next, the N–C bond was broken to form 4-aminobenzene sulfonamide, which was ultimately degraded into aniline. However, PCS had no impact on the N–C bond breaking, with no difference observed in the relative abundance of 4-aminobenzene sulfonamide (Supplementary Fig. S2–S5). In Pathway II, due to the oxygen exchange that occurred during the input of the domestic sewage, SMX was first metabolized into 3-Amino-5-methylisoxazole (3A5MI) and 4-aminobenzene sulfinic acid, the main products of aerobic SMX degradation [34]. 3A5MI was then converted to 5-methylisoxazole via oxidation and deamination and subsequently degraded to isopropanol. PCS promoted S–N bond rupture and 3A5MI deamination. Significantly, a high PCS concentration inhibited 3A5MI deamination, as evidenced by the lower relative abundance of 5-methylisoxazole (the downstream product of 3A5MI) caused by B300V compared to B100V. Moreover, in B100DV, 3A5MI was not detected, and 5-methylisoxazole reached its highest relative abundance, indicating that 3A5MI degradation was accelerated by DPCS. In Pathway III, benzene sulfinic acid was formed by deamination of 4-amino benzenesulfinic acid, then oxidized to phenylthiol and degraded into small molecules (e.g., methane and carbon dioxide). Benzenesulfonic acid was detected only in B300V, indicating that the high PCS concentration may have inhibited the conversion of benzene sulfinic acid into phenylthiol.

3.2. Viruses affected the EPS content

The lower SMX content observed in the sediments treated with PCS may have resulted from enhanced microbial degradation of extractable SMX residues. PCS also altered the EPS composition (Supplementary Text S6), which may, in turn, influence SMX removal. Overall, the low-concentration PCS increased EPS production (Supplementary Fig. S6) and microbial regulation of SMX removal. Bacteriophages have been shown to promote microbial adaptability under environmental stress by enriching AMGs involved in EPS synthesis [35,36]. They have also been reported to act as naturally occurring, environmentally friendly biofilm repair agents by secreting lytic enzymes that degrade EPS [37]. This delays the formation of overly thick EPS layers and thus enhances nutrient supply within the biofilm and access to external nutrients or oxygen, which are key factors for SMX removal. Interestingly, high-concentration PCS and DPCS reduced EPS generation, indicating that PCS regulated biofilm structure. These findings provide a novel reference for microbial renewal and a solution to biological blockage problems in sewage treatment systems.

3.3. Adding the PCS optimized virus–bacteria interactions

Across treatments, 23,299–68,070 viral contigs were identified. These contigs clustered into 4191 VCs (approximating genus-level groupings), and only 15 viral contigs were classified as giant viruses (>200 kb; Supplementary Table S4). PCS addition increased the number of viral contigs and community richness scores, but was associated with lower diversity as measured by the Shannon and Simpson indexes (Fig. 3a). PCA showed significant separation among the treatment systems and obvious aggregation among the replicates (Fig. 3b). Compared with B100V, both B300V and B100DV had more viral contigs and greater community diversity and richness. These results indicated that high-concentration PCS and PCS derived from sediment pre-incubated with SMX had positive effects on viral colonization in SMX-stressed sediments.

The viral community was clearly different in treatments containing PCS ($R = 1$, $p = 0.001$, Fig. 3c). Across systems, we detected 68–106 viral types, with 34 VCs shared across the systems (Fig. 3d). Similar to the distribution of the viral contigs, viral-type richness was higher in B100V, B300V, and B100DV. B300V ($n = 104$) and

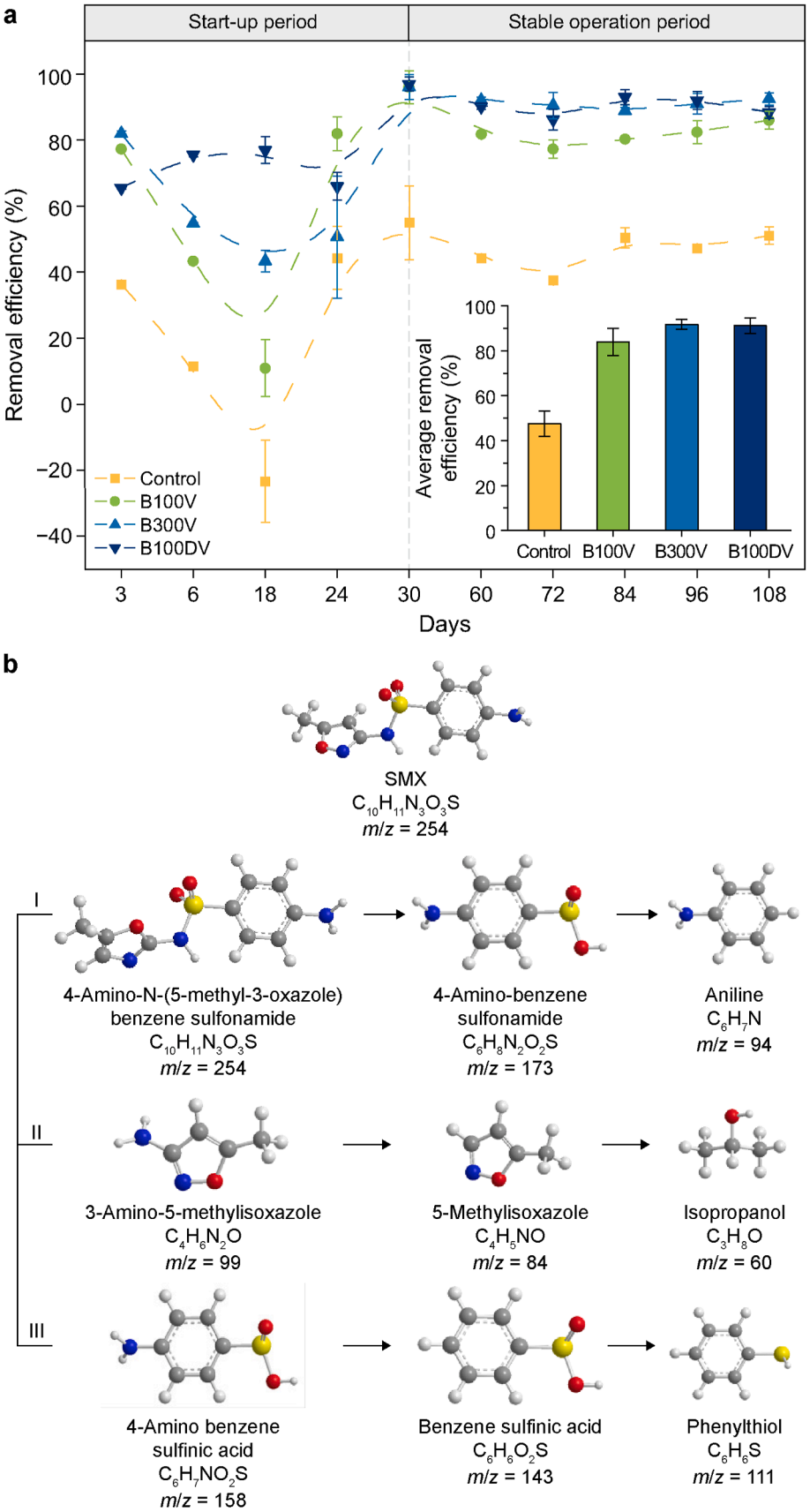

Fig. 2. Effect of phage-concentrated solution addition on sulfamethoxazole (SMX) removal. a, SMX removal efficiencies in different systems. The figure inserted shows the average removal efficiency of SMX. **b**, Possible SMX degradation pathways.

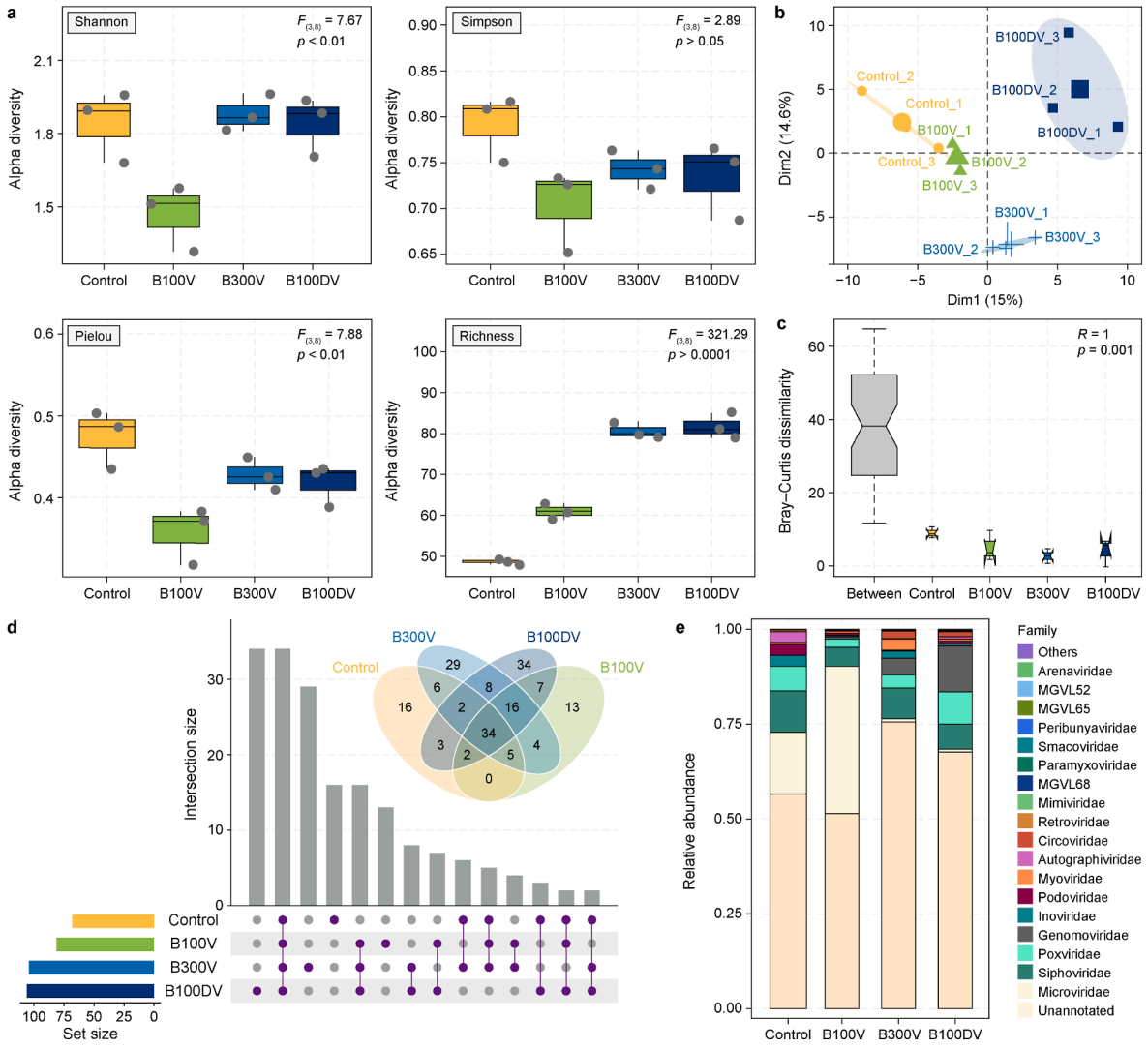

Fig. 3. The composition and diversity of the viral community. **a**, The alpha diversity of the viral community. The median line represents the median of the dataset. Each point represents a sample, and the overlaid boxplot summarizes the data distribution for each group. Error bars represent the standard deviation. **b**, Principal components analysis comparing differences in community composition. **c**, The interspecific differences based on Bray–Curtis distance. "Between" represents the distribution of dissimilarities between samples from different groups. **d**, UpSet plot of intersections (top) and set sizes (left) for viral clusters (VCs) across treatments, with VCs defined by vConTACT2 (v2.0). Columns denote set intersections defined by the dot matrix below; bars indicate intersection size (number of VCs), and horizontal bars show set size for each treatment. **e**, The viral taxonomic composition at the family level.

B100DV ($n = 106$) showed similar viral profiles and shared 60 VCs. Notably, B100DV contained 34 unique VCs, indicating that environmental stressors, such as SMX contamination, can cause genetic variation in viruses [21].

Family-level profiling (Fig. 3e) showed that unannotated viruses dominated in all samples, with relative abundances of 51.4–75.6%. Among annotated families, Microviridae, Siphoviridae, and Poxviridae were most abundant in the control and B100V, consistent with reports from clean and organochlorine-contaminated soils [5]. Compared with the control, B100V showed a 22.4% higher relative abundance of Microviridae (38.8%), whereas Siphoviridae and Poxviridae decreased by 4.9% and 2.2%, respectively. Dominant viral families varied with the concentration and type of PCS. In B300V and B100DV, Siphoviridae, Poxviridae, and Genomoviridae were predominant, but their relative abundances differed (B300V: 8.1%, 3.4%, and 4.4%; B100DV: 6.6%, 8.6%, and 12.0%, respectively). Viral concentration and types shaped viral community structure and richness in response to SMX stress. The high relative abundance of Siphoviridae may be relevant to SMX removal, as the dihydrofolate reductase enzyme encoded by Siphoviridae bacteriophage AXL1 has been shown to induce resistance to SMX [38].

Viruses can regulate the structure and function of their hosts, thereby influencing host resistance to pollutant stressors and pollutant transformation. Among the identified viral contigs, 36,295 (18.6%) were annotated to hosts. Of these, 31 viruses were linked with 20 bacterial host phyla and 747 host species (Supplementary Table S5). At the species level, PCS affected the variety of hosts. More specifically, 19 viral contigs were linked to 13 host phyla and 305 species in the control, 15 viruses were linked to 16 host phyla and 395 species in B100V, 19 viral contigs were linked to nine host phyla and 421 species in B100DV, and 21 viral contigs were linked to nine host phyla and 449 species in B300V.

At the phylum level, Proteobacteria were the most common hosts, followed by Firmicutes, Actinobacteria, Euryarchaeota, and Bacteroidetes (Fig. 4a). These phyla represented the dominant

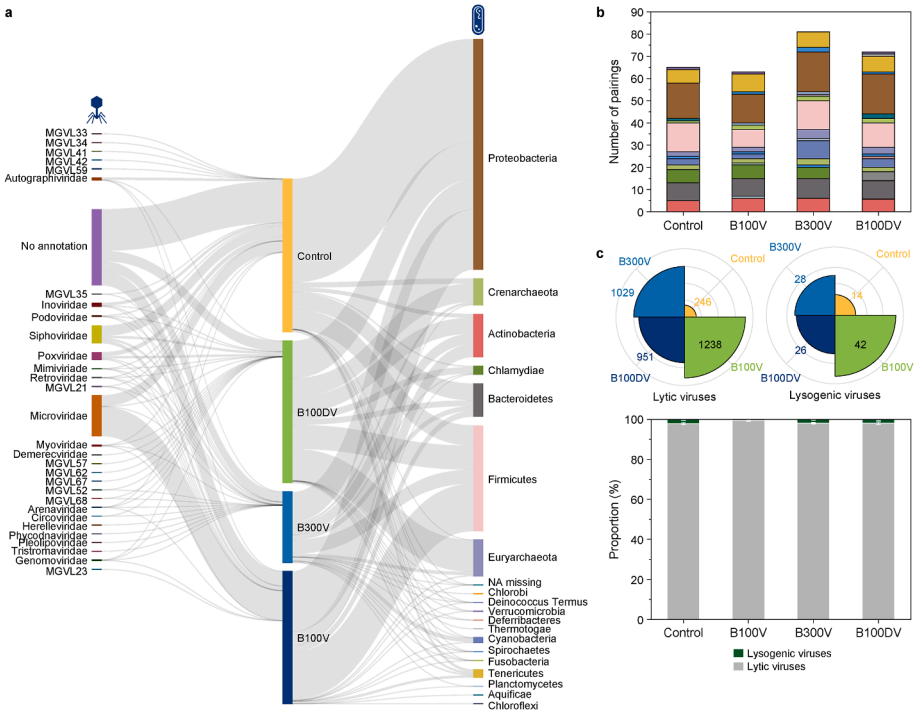

Fig. 4. Analysis of interactions between viruses and their hosts. a, Predicted virus–host associations. Left: the viral contigs that can match the host; Middle: the names of different samples; Right: the distribution of bacterial hosts at the phylum level. **b**, The number of virus–host pairs per sample and the corresponding host classifications are consistent with those shown in panel **a**. **c**, The number and proportion of lytic or lysogenic viruses in different systems.

members of the bacterial community, and they are also reportedly the most common in deep sea sediments, soils, and activated sludge from wastewater treatment plants [26,35,39]. The relative abundance of viral hosts at the phylum level was also influenced by PCS concentration and type. For example, compared with those in the control, the relative abundances of Proteobacteria, Firmicutes, and Bacteroidetes were all lower in B300V and B100DV, while the levels of Euryarchaeota and Crenarchaeota were higher (Supplementary Fig. S7). In addition, the relative abundance of some host species (e.g., Actinobacteria, Chlamydiae, and Cyanobacteria) differed between B300V and B100DV. The presence of the PCS changed the pattern of coexistence between viruses and bacteria under SMX stress. Across the four treatments, we identified 281 virus–host pairs. Pair counts were similar in the control ($n = 65$) and B100V ($n = 63$) (Fig. 4b). By contrast, B300V ($n = 72$) and B100DV ($n = 81$) yielded more pairs than B100V, suggesting higher apparent infectivity under higher PCS dose and when PCS was derived from SMX-incubated sediment. Consistently, these treatments showed higher abundances of anti-phage defense systems (Supplementary Table S6), indicating increased viral predation pressure on bacterial hosts.

Phage-concentrated solution affected the composition of the sediment virome in terms of the abundance of lytic and lysogenic viruses. Lytic viruses dominated the viral community (97.6–99.7% relative abundance) and were significantly more abundant than lysogenic viruses ($p < 0.05$; Fig. 4c). The coexistence of lytic and lysogenic viruses is a natural outcome of the chaotic population dynamics that arise within a sufficiently diverse community, wherein obligate lytic viruses typically outcompete lysogenic viruses [36]. Lytic viruses tend to lyse their host bacterial cells and generate a burst of viral progeny, while lysogenic viruses integrate their genomes into the bacterial host DNA and improve survivability of the host [40]. In this study, lytic viruses remained dominant under SMX exposure coexisted with lysogenic viruses. A balance between lytic and lysogenic viruses has been associated with greater microbial community stability and resilience to pollution stress [36]. PCS addition increased the proportion of lytic viruses, indicating that viral composition responds to viral concentration and type. Lysogenic viruses accounted for 1.92% of the viruses in B100DV and 1.88% in B300V. Notably, under deteriorating conditions, lysogenic strains can outcompete obligate lytic strains [36].

3.4. PCS improved bacterial adaptability and metabolic capacity

The bacterial diversity and evenness in the sediments was decreased (Fig. 5a), which might be related to the infections of lytic viruses to host cells host cells [41]. Increasing PCS concentration had little impact on the bacterial diversity and evenness ($p > 0.05$). However, DPCS significantly reduced both metrics ($p < 0.01$), consistent with higher infectivity of the viruses.

The addition of PCS changed the bacterial community composition in the sediments (Fig. 5b and c). At the phylum level (Fig. 5d), Proteobacteria (84.5%), Firmicutes (5.3%), and Bacteroidetes (7.9%) were dominant in the control, accounting for 97.7% of the total bacterial abundance. Species in these phyla were also ranked as the most important SMX-degrading bacteria [42–44]. In contrast, the relative abundances of Proteobacteria (91.7%) and Firmicutes (5.6%) were higher in B100V, while the level of Bacteroidetes (0.8%) was significantly lower (these three phyla accounted for 98.1% of the total bacterial abundance; $p < 0.05$). The relative abundances of these three phyla were different when the PCS concentration was increased or when the PCS was derived from sediment pre-incubated with SMX (B300V: 64.0%, 4.0%, and 27.6%; B100DV: 32.1%, 3.1%, and 53.3%). Notably, Euryarchaeota were enriched in sediments treated with the PCS, with relative abundances of 0.7%, 4.3%, and 11.5% in B100V, B300V, and B100DV, respectively. Euryarchaeota was the most abundant lineage of

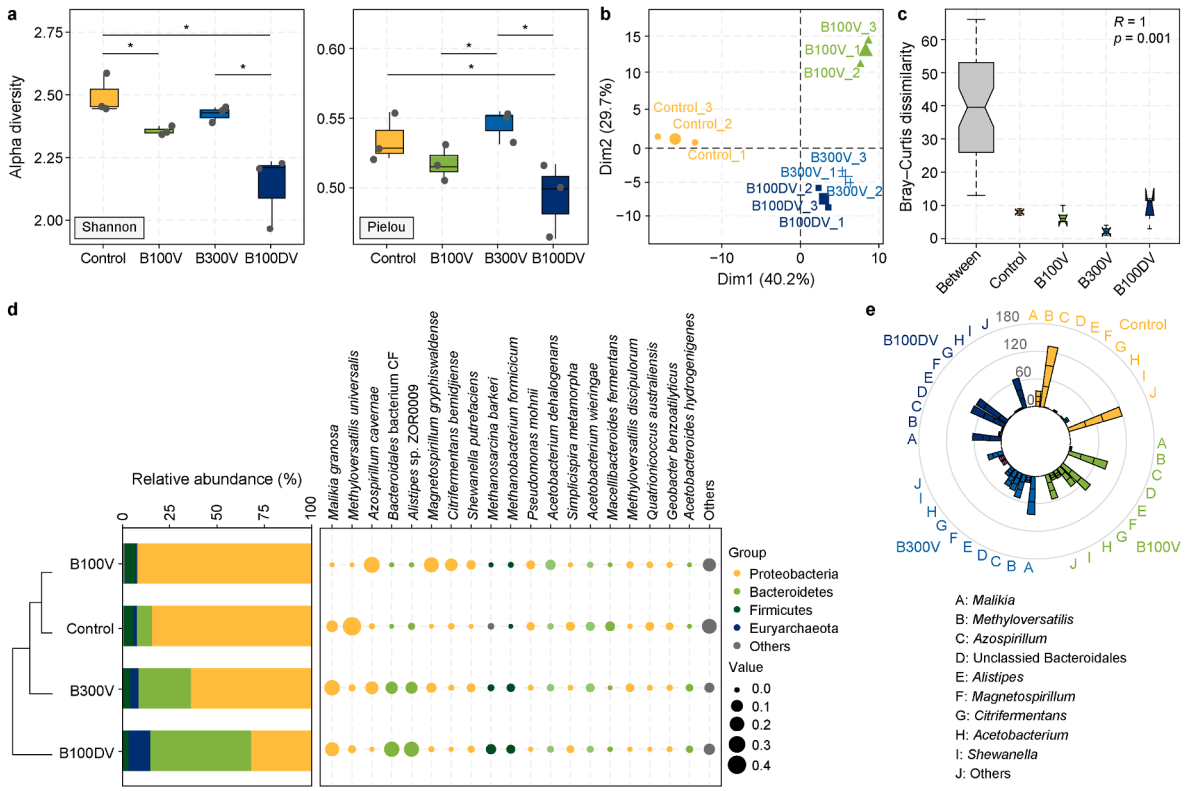

Fig. 5. Bacterial community composition and diversity. a, Alpha diversity of bacterial community. Error bars represent the standard deviation. Asterisks denote the significance level based on F-tests: *$p < 0.05$. **b**, Principal components analysis of bacteria based on the relative abundance of species. **c**, The interspecific differences based on Bray–Curtis distance. "Between" represents the distribution of dissimilarities between samples from different groups. **d**, The relative abundance of the top 20 abundant bacterial species and phylum. **e**, The bacterial community composition at the genus level.

Archaea and the main viral–host phylum [26].

At the genus level (Fig. 5e), *Magnetospirillum* was the most abundant in the control (43.5%) but occurred at lower relative abundance in PCS-amended treatments. *Magnetospirillum* has been reported to contain genes associated with the activation of carbonaceous organics and small-molecular organic acids involved in pyruvate degradation, which can provide energy for SMX removal [45]. The addition of PCS decreased the relative abundance of *Malikia* (0.01% in B100V vs. 11.0% in the control). Increasing the PCS concentration and incubating the PCS increased the relative abundance of *Malikia* (27.1% in B300V vs. 20.7% in B100DV). *Malikia* reportedly contributes to the degradation of aromatic compounds [46], which might substantially facilitate SMX removal. Unclassified Bacteroidetes was the most abundant bacterial type in B100DV (26.2%). *Bacteroidales* have been shown to correlate positively with viral presence and are considered suitable indicators of viral contamination of water bodies [47]. Moreover, some electroactive bacteria, such as *Geobacter* (0.3–2.2%) and *Shewanella* (0–5.2%), were found in samples treated with the PCS. This indicated that the PCS may have accelerated the electron transfer rate within the sediment, thereby promoting SMX removal. Conversely, the relative abundance of these species was lower in B300V and B100DV. Overall, the PCS type and concentration impacted the microbial community structure and function. Notably, the dominant SMX-degrading bacteria shifted from Proteobacteria to Bacteroidetes, particularly in B100DV.

Furthermore, increasing the concentration of PCS induced bacterial colonization [48], thereby improving bacterial adaptability. Network analyses showed that, relative to the control, bacterial community and virus–bacteria interactions were weaker in B100V (Supplementary Fig. S8 and S9), with fewer nodes and edges. Virus–bacteria coordination was weakened by the PCS, with the proportion of positive correlations between viruses and bacteria decreasing from 57.6% (control) to 53.5% (B100V). However, the strength of the bacterial community interactions and the virus–bacteria interactions was higher in B300V and B100DV. The proportion of positive correlations was 50.9% in B300V and 58.4% in B100DV. These results suggest that DPCS had beneficial effects on microbial survival and community stability.

Viruses can assist bacteria in responding to SMX stress by regulating metabolic processes that support the host bacterium's survival and nutrient cycling. The metabolic capacity of sediment bacteria was improved by the addition of PCS. Specifically, B100V showed enrichment of metabolic pathways related to bacterial survival (e.g., replication and repair, membrane transport, transport and catabolism, and signaling molecules and interaction) and energy production (e.g., carbohydrate metabolism, biosynthesis of other secondary metabolites, glycan biosynthesis and metabolism, and metabolism of terpenoids and polyketides) (Supplementary Fig. S10a). This indicates that the PCS enhanced bacterial survival under SMX stress. This finding aligns with previous studies that viruses help bacteria survive under benzo[a]pyrene or organochlorine stress [4,5]. Moreover, the diversity and richness of genes related to element cycling (i.e., carbon, nitrogen, phosphorus, and sulfur cycling) were altered by the PCS (Supplementary Fig. S10b). While the number of each gene was higher when the PCS was added, the relative abundances of them were decreased (Supplementary Fig. S10c).

3.5. Virus-encoded AMGs played an important role in SMX degradation

The number and types of virus-encoded AMGs were shaped by the viruses present [40]. Furthermore, AMGs modulated the metabolism of the host bacteria and microbial-driven biogeochemical processes. The number of AMGs detected in the control was 26, whereas 275 AMGs were detected in B100V (Fig. 6a). Compared with B100V, fewer AMGs were detected in B100DV ($n = 137$) and B300V ($n = 161$), and there were 14 fewer AMG types in B100DV (Fig. 6b). The relative abundance of AMGs encoded by lytic viruses decreased by 24.1% when PCS was derived from 100 g sediment pre-incubated with SMX (Supplementary Fig. S11) due to the enrichment of certain AMGs under SMX stress. Moreover, only eight AMG types were shared across the four systems, indicating that the PCS type and concentration affected the AMGs' function and role. Furthermore, viral communities with different proportions of lytic and lysogenic viruses tend to mediate microbial-driven biogeochemical cycles via AMGs in different ways. The relative abundance of lytic virus-encoded AMGs was higher than that of lysogenic virus-encoded AMGs across the four systems (Supplementary Fig. S11). Given that this type of ratio has been shown to improve host translation efficiency and viral progeny reproduction [49], it likely facilitated the degradation and transformation of SMX in this study. Hence, the high-concentration PCS and DPCSs influenced the AMG composition. In addition, PCS (at low concentration) accelerated the degradation and transformation of SMX by increasing the number and diversity of AMG.

The metabolic pathways associated with the virus-encoded AMGs were enriched for amino acid metabolism, biosynthesis of other secondary metabolites, carbohydrate metabolism, metabolism of cofactors and vitamins, metabolism of terpenoids and polyketides, glycan biosynthesis and metabolism, and energy metabolism (Fig. 6a). The AMGs related to microbial metabolism and energy production may be involved in SMX degradation and transformation. In particular, the AMGs related to folate biosynthesis, which is associated with cofactor and vitamin metabolism, were ranked as the most common [50], representing nine, six, and five annotated genes (e.g., *que*C/D/E/F) in B100V, B300V, and B100DV, respectively, while they were not detected in the control (Supplementary Fig. S12). Additionally, these AMGs were enriched in B100DV, indicating that DPCS was more effective at alleviating ROS, as folate has potent antioxidant properties [51]. Other AMGs associated with cell membrane integrity and robustness were detected, namely *lpx*D (B100V), *van*Y (B300V), and *NEU*1 (B100DV), with relative abundances of 4.1%, 0.01%, and 3.9%, respectively.

AMGs related to element cycling (e.g., carbon, nitrogen, and sulfur cycling) enhanced the host bacteria's competitiveness for nutrients. Sediment is generally rich in nutrients, especially polysaccharides and organic sulfur compounds derived from animals and plants (Fig. 6c).

AMGs associated with several polysaccharide metabolism processes (i.e., amino sugar and nucleotide sugar metabolism, fructose and mannose metabolism, galactose metabolism, pentose and glucuronate interconversions, arabinogalactan biosynthesis—mycobacterium, lipopolysaccharide biosynthesis, N-glycan biosynthesis, and polyketide sugar unit biosynthesis) were significantly enriched when the PCS was added, especially in B100V ($p < 0.05$). The findings of a previous study suggest that increased abundances of these AMGs are associated with the generation of amino sugars and their release via cell lysis [52]. Amino sugars are a major constituent of the bacterial cell wall and can accumulate in the short term due to cell lysis caused by viral infection. In addition, these compounds can supply adenosine triphosphate for the bacterial

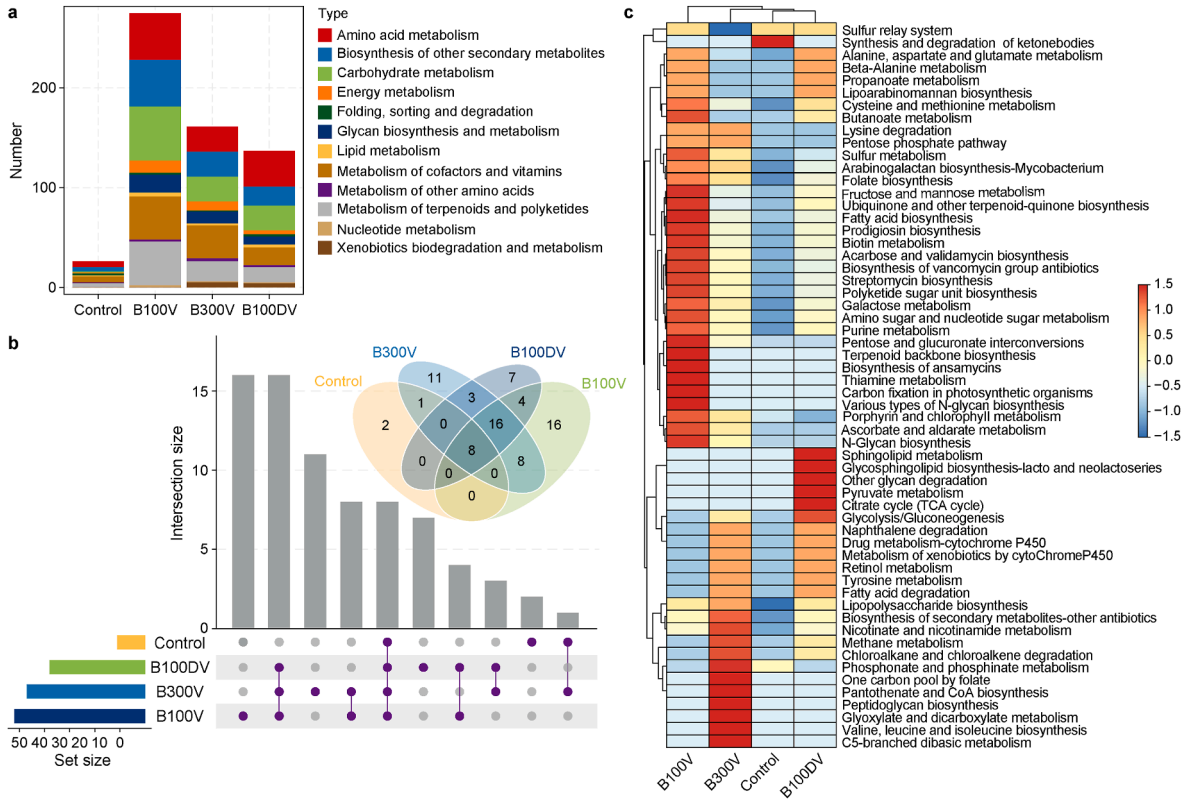

Fig. 6. Virus-encoded auxiliary metabolic genes (AMGs). **a**, The number of AMGs in different systems. **b**, UpSet plot of intersections (top) and set sizes (left) for AMGs types across treatments, with AMGs defined by VIBRANT. Columns denote set intersections defined by the dot matrix below; bars indicate intersection size (number of AMGs), and horizontal bars show set size for each treatment. **c**, Heatmap shows the AMG compositions based on the KEGG L3 pathway.

metabolism of SMX. Some AMGs associated with cellulose synthase (*bcs*A), lipopolysaccharide biosynthesis (*lpx*ADH), polysaccharide biosynthesis (*alg*A), and EPS (*rfb*ABCD) are reportedly involved in biofilm formation [53]. In our study, the relative abundance of *lpx*AD, *alg*A, and *rfb*ABCD increased with the addition of the PCS. Among these AMGs, *rfb*B showed the highest relative abundance, indicating that viruses played an important role in regulating the EPS structure. However, increasing the PCS concentration was more effective than using DPCS.

The AMG *cys*H encodes an enzyme involved in the assimilatory sulfate reduction pathway that catalyzes the reduction of phosphoadenylyl sulfate to sulfite [48]. This AMG was detected in B100V (relative abundance: 6.7%), B300V (1.0%), and B100DV (0.4%). Its relatively higher abundance in B100V was attributed to sulfate assimilation and the direct sulfonation of organic molecules [54]. Viral *cys*H has been ubiquitously detected in marine, freshwater, soil, engineered, human, wetland, and thermal spring microbiomes [55].

3.6. PCS decreased the abundance of ARGs

The relative abundances of ARGs harbored by bacteria and viruses changed upon PCS addition. Overall, the abundance of ARGs decreased (Supplementary Fig. S13a). Compared with the control (2299.6 coverage), the total ARG abundance in B100V (989.7 coverage) decreased by 57.0%, which was not significantly different from that in B300V (993.5 coverage) ($p > 0.05$). Notably, DPCS had a more pronounced negative effect on ARG abundance, with a total ARG abundance of 933.5 coverage in B100DV. Viruses in the environment are often hosted by bacteria that carry ARGs, and more than half of them are lytic in nature [56], while the contribution of lysogenic virus-mediated transduction is relatively low. In our study, lytic viruses were dominant across all systems, while the proportion of ARGs carried by lysogenic viruses was <0.2% (Supplementary Fig. S13b), indicating that the viral community played a greater role in the lysis of antibiotic-resistant bacteria than in ARG proliferation [13,57]. DPCS had a more significant negative effect on the ARGs, while the PCS concentration showed no significant effect.

In the control, we detected 17 ARG types and 132 ARG subtypes carried by bacteria (Fig. 7a). The dominant types were multidrug (35.5%), bacitracin (15.2%), and sulfonamide (11.4%) ARGs (Fig. 7b). The ARG diversity increased with the addition of the PCS, with 18 ARG types and 144 ARG subtypes carried by bacteria detected in B100V. The relative abundance of multidrug ARGs significantly increased to 49.5% ($p < 0.05$), while that of sulfonamide ARGs

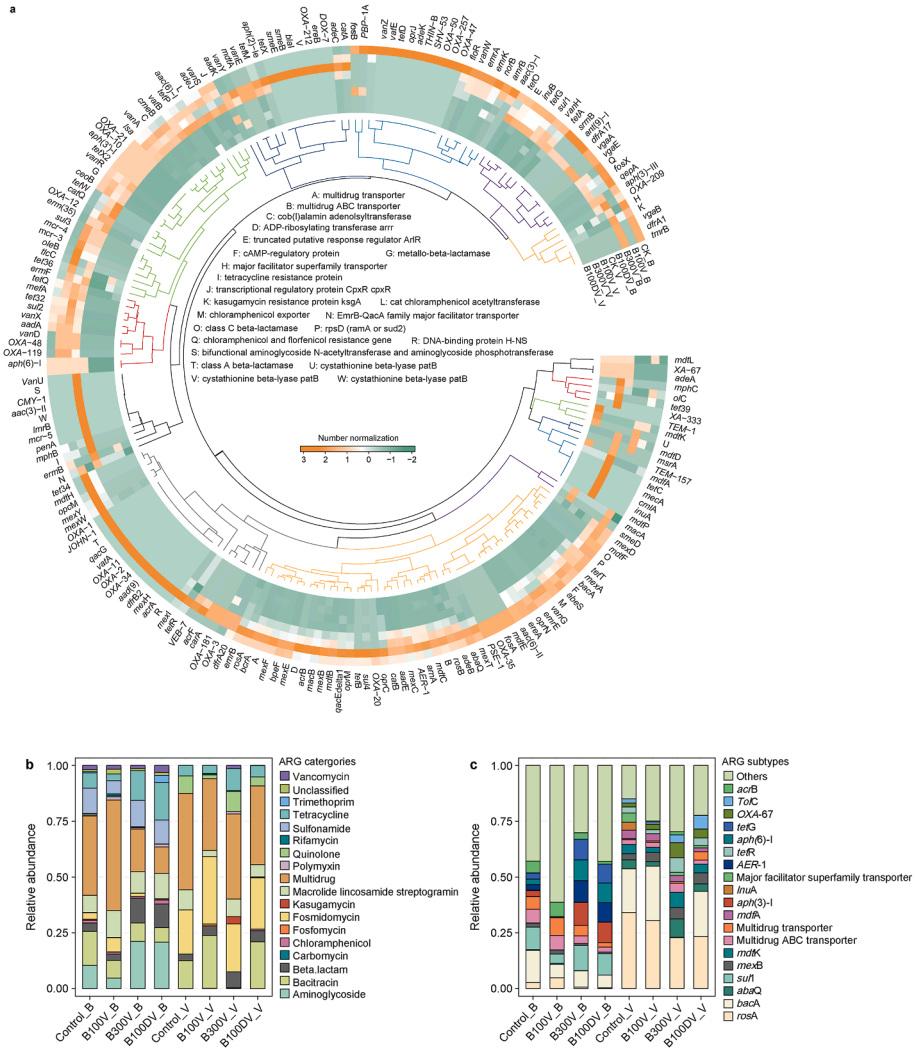

Fig. 7. The antibiotic resistance genes (ARGs) composition carried by bacteria (B) and viruses (V) as phage concentrated solutions added. **a**, The number of ARG subtypes. **b**, The composition of ARG types. **c**, The relative abundance of the top 20 abundant ARG subtypes.

decreased to 6.01%. PCS addition increased the ARG diversity by inducing non-corresponding ARG types and reducing corresponding ARG types. Compared with B100V, the relative abundance of multidrug ARGs (19.1%) was reduced and the relative abundance of sulfonamide ARGs (11.3%) increased when the PCS concentration was higher. However, compared with B100V, the ARG diversity decreased with the addition of DPCS; 16 ARG types and 122 ARG subtypes were detected in B100DV. This result may be related to the antibiotic's specific selectivity under SMX stress. The most dominant types in B100DV were aminoglycoside (20.8%), tetracycline (16.8%), and multidrug (11.8%) ARGs. Compared with B100V, B100DV exhibited a higher relative abundance of sulfonamide ARGs (10.8%). Thus, viruses affected the total ARG abundance and the ARG types and subtypes.

Bacteria-carried ARG subtypes differed between the control and B100V (Fig. 7c). The most common subtypes were *bac*A (14.4%), *sul*1 (10.1%), and multidrug ABC transporter (6.2%) in the control; and multidrug transporter (7.9%), multidrug ABC transporter (6.5%), and *acr*B (6.5%) in B100V. The relative abundance of *sul*1 was 5.9% lower in B100V than in the control, whereas *sul*1 in B100DV was higher than in B100V but remained below the control level. These results indicate that DPCS promoted ARG proliferation, and the ARG transfer activity induced by DPCS was reduced compared to that in the control. However, the relative abundance of *sul*1 increased with the PCS concentration (11.3% in B300V). Therefore, it is crucial to choose the appropriate PCS concentration and type when planning to regulate ARG abundance using viruses.

3.7. Identification of direct and indirect drivers of SMX removal

In wetland sediment, SMX removal is influenced by the composition of the microbial community. We used MRM to clarify the relative contributions of the bacterial and viral communities to SMX removal (Fig. 8a). The overall differences in SMX removal were best explained by the bacterial and viral communities ($R^2 = 1$, $p < 0.05$). In the first MRM analysis, the phyla Proteobacteria, Euryarchaeota, and Firmicutes had larger partial regression coefficient values ($|b| = 8.17$, 4.50, and 23.60, respectively), while the phylum Bacteroidetes had a smaller but significant partial regression coefficient ($|b| = 0.47$). In the second MRM analysis, *Siphoviridae*, *Genomoviridae*, *Poxviridae*, and *Microviridae* all had a larger effect on SMX removal ($|b| = 10.19$, 7.98, 5.50, and 2.87, respectively) than the unannotated viruses ($|b| = 0.11$).

To explore the direct and indirect impacts of the PCS on SMX removal, we used RFM to identify the most influential functional metabolic pathways in bacteria and viruses (Supplementary Fig. S14). In bacteria, the most abundant functional metabolic pathways were the excretory system, xenobiotic biodegradation

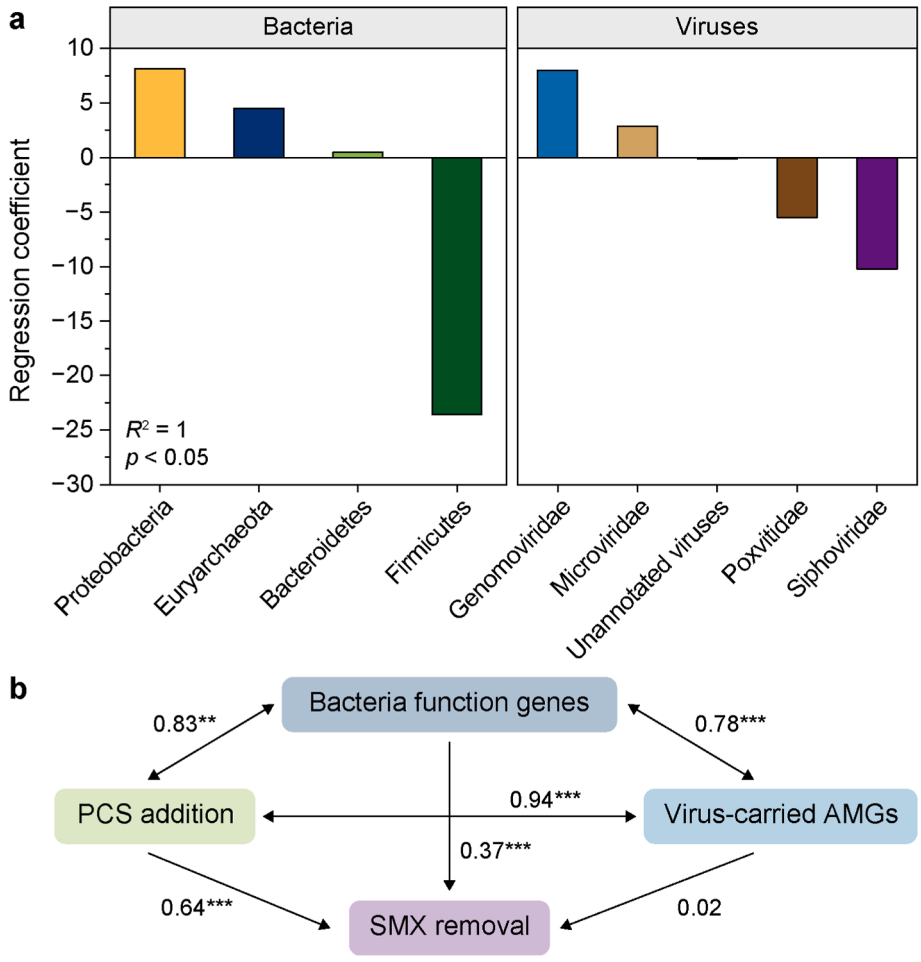

Fig. 8. Effect of phage-concentrated solutions (PCS) addition on sulfamethoxazole (SMX) removal and sediments multifunctionality. **a**, The results of the multiple regression model analysis. The first model results were calculated using bacterial communities as predictors, while the second used viral communities. **b**, Structural equation model. Model fit: Chi-square = 4.921; $p = 0.178$; goodness-of-fit index = 1.000; comparative fit index = 0.979; standard root mean-square residual = 0.018; root mean square error of approximation = 0.231. Significant levels: *$p < 0.05$, **$p < 0.01$, ***$p < 0.001$. Numbers adjacent to arrows indicate path coefficients. AMGs: auxiliary metabolic genes.

and metabolism, environmental adaptation, viral protein families, and genes of unknown function. In viruses, the most abundant functional metabolic pathways were cell growth and death, metabolism protein families, genetic information processing (unclassified), amino acid metabolism, and aging. These results indicated that the PCS influenced bacterial adaptability and metabolic capacity.

We then used SEM to analyze the effects of PCS addition on SMX removal and microbial function in wetland sediments (Fig. 8b). SMX removal, bacterial function and metabolism, and viral function and metabolism were all significantly improved by PCS addition ($p < 0.05$). Bacterial metabolism showed a significant positive correlation with viral metabolism ($p < 0.001$), suggesting that viruses may promote coevolution between bacteria and viruses in wetland sediments. However, there was no significant association between virus-carried AMGs and SMX removal ($p > 0.05$). Thus, it appears that PCS affected bacterial metabolism by enriching virus-encoded AMGs. Together, these findings indicate that the PCS indirectly enhanced SMX removal by enriching virus-encoded AMGs and bacterial metabolism. The viruses effectively redirected the metabolic processes of the host bacteria.

4. Conclusion

In this study, virus–bacteria interactions and virus-encoded AMGs facilitated microbial adaptation to SMX stress in wetland sediment. PCS addition significantly increased EPS secretion and enriched degradation bacteria, functional genes related to microbial adaptability, and AMGs. Positive virus–bacteria interactions improved SMX removal, and viruses reduced bacterial resistance and the corresponding ARG types by lysing antibiotic-resistant bacteria. Moreover, the concentration and type of PCS significantly affected the virus–bacteria interactions. Collectively, our findings indicate that viruses play an important ecological role for viruses in shaping microbial responses to pollutant stress and highlight their potential to enhance bioremediation in wetland sediments. Our findings provide a theoretical foundation for reducing the environmental and health risks associated with antibiotics and ARGs.

CRediT authorship contribution statement

Ying Liu: Writing – review & editing, Writing – original draft, Software, Methodology, Investigation, Data curation, Conceptualization. **Xiaomeng Wei:** Writing – original draft, Validation, Supervision, Methodology, Investigation, Conceptualization. **Maozhen Han:** Writing – review & editing, Visualization, Software, Methodology, Formal analysis, Data curation. **Boyu Li:** Writing – review & editing, Visualization, Methodology, Investigation, Formal analysis, Data curation. **Shaoyong Lu:** Resources, Investigation, Formal analysis. **Haiming Wu:** Resources, Methodology, Investigation, Formal analysis, Data curation. **Xiaohui Liu:** Writing – review & editing, Validation, Funding acquisition, Data curation, Conceptualization. **Fengchang Wu:** Software, Resources, Methodology, Formal analysis, Data curation.

Declaration of competing interest

The authors declare that they have no known competing financial interests or personal relationships that could have appeared to influence the work reported in this paper.

Acknowledgements

This work was financially supported by the National Natural Science Foundation of China (NSFC) (No. 42207260, 82300645), the Taishan Scholars Project of Shandong Province (No. tsqn202312094, tsqnz20250721), Shandong Provincial Higher Education Institution Youth Innovation Teams (No. 2023KJ034), Outstanding Youth Program of Anhui Provincial Natural Science Foundation (2408085Y039), Key Project for cultivating outstanding young teachers of Higher Education in Anhui Province (YQZD202406).

Appendix A. Supplementary data

Supplementary data to this article can be found online at https://doi.org/10.1016/j.ese.2026.100698.

Data availability

Data will be made available on request. The raw sequence data generated in this study have been deposited in NCBI with accession number of PRJNA1176300.

References

[1] Y. Kuzyakov, K. Mason-Jones, Viruses in soil: nano-scale undead drivers of microbial life, biogeochemical turnover and ecosystem functions, Soil Biol. Biochem. 127 (2018) 305–317, https://doi.org/10.1016/j.soilbio.2018.09.032.
[2] A. Chevallereau, B.J. Pons, S. van Houte, E.R. Westra, Interactions between bacterial and phage communities in natural environments, Nat. Rev. Microbiol. 20 (2022) 49–62, https://doi.org/10.1038/s41579-021-00602-y.
[3] X. Tang, P. Yu, L. Tang, M. Zhou, C. Fan, Y. Lu, J. Mathieu, W. Xiong, P.J. Alvarez, Bacteriophages from arsenic-resistant bacteria transduced resistance genes, which changed arsenic speciation and increased soil toxicity, Environ. Sci. Technol. Lett. 6 (2019) 675–680, https://doi.org/10.1021/acs.estlett.9b00600.
[4] R. Xia, M. Sun, J.L. Balcazar, P. Yu, F. Hu, P.J.J. Alvarez, Benzo a pyrene stress impacts adaptive strategies and ecological functions of earthworm intestinal viromes, ISME J. 17 (2023) 1004–1014, https://doi.org/10.1038/s41396-023-01408-x.
[5] X. Zheng, M.T. Jahn, M. Sun, V.-P. Friman, J.L. Balcazar, J. Wang, Y. Shi, X. Gong, F. Hu, Y. Zhu, Organochlorine contamination enriches virus-encoded metabolism and pesticide degradation associated auxiliary genes in soil microbiomes, ISME J. 16 (2022) 1397–1408, https://doi.org/10.1038/s41396-022-01188-w.
[6] J. Cui, L. Fu, B. Tang, L. Bin, P. Li, S. Huang, F. Fu, Occurrence, ecotoxicological risks of sulfonamides and their acetylated metabolites in the typical wastewater treatment plants and receiving rivers at the Pearl River Delta, Sci. Total Environ. 709 (2020) 136192, https://doi.org/10.1016/j.scitotenv.2021.147811.
[7] X. Liu, S. Lu, W. Guo, B. Xi, W. Wang, Antibiotics in the aquatic environments: a review of lakes, China, Sci. Total Environ. 627 (2018) 1195–1208, https://doi.org/10.1016/j.scitotenv.2018.01.271.
[8] Y. Yang, X. Zhang, J. Jiang, J. Han, W. Li, X. Li, K.M.Y. Leung, S.A. Snyder, P.J.J. Alvarez, Which micropollutants in water environments deserve more attention globally? Environ. Sci. Technol. 56 (2022) 13–29, https://doi.org/10.1021/acs.est.1c04250.
[9] J. Xu, G. Sheng, Y. Ma, L. Wang, H. Yu, Roles of extracellular polymeric substances (EPS) in the migration and removal of sulfamethazine in activated sludge system, Water Res. 47 (2013) 5298–5306, https://doi.org/10.1016/j.watres.2013.06.009.
[10] Q. Wang, L. Geng, Z. Gao, Y. Sun, X. Li, S. Sun, Y. Luo, Microalgae enhances the adaptability of epiphytic bacteria to sulfamethoxazole stress and proliferation of antibiotic resistance genes mediated by integron, Environ. Sci. Technol. 58 (2024) 19397–19407, https://doi.org/10.1021/acs.est.4c04925.
[11] Z. Li, R. Cheng, F. Chen, X. Lin, X. Yao, B. Liang, C. Huang, K. Sun, A. Wang, Selective stress of antibiotics on microbial denitrification: inhibitory effects, dynamics of microbial community structure and function, J. Hazard Mater. 405 (2021) 124366, https://doi.org/10.1016/j.jhazmat.2020.124366.
[12] H. Li, H. Xu, H. Song, Y. Lu, X. Yang, Antibiotic resistance genes, bacterial communities, and functions in constructed wetland-microbial fuel cells: responses to the co-stresses of antibiotics and zinc, Environ. Pollut. 265 (2020) 115084, https://doi.org/10.1016/j.envpol.2020.115084.
[13] J. Zhang, T. Lu, Y. Song, U.N.d. Rocha, J. Liu, M. Nikolausz, Y. Wei, H.H. Richnow, Viral communities contribute more to the lysis of antibiotic-resistant bacteria than the transduction of antibiotic resistance genes in anaerobic digestion revealed by metagenomics, Environ. Sci. Technol. 58 (2024) 2346–2359, https://doi.org/10.1021/acs.est.3c07664.
[14] H. Liao, C. Liu, S. Zhou, C. Liu, D.J. Eldridge, C. Ai, S.W. Wilhelm, B.K. Singh, X. Liang, M. Radosevich, Q.-e. Yang, X. Tang, Z. Wei, V.-P. Friman, M. Gillings, M. Delgado-Baquerizo, Y.-g. Zhu, Prophage-encoded antibiotic resistance genes are enriched in human-impacted environments, Nat. Commun. 15 (2024) 8315, https://doi.org/10.1038/s41467-024-52450-y.

[15] L.P.P. Braga, A. Spor, W. Kot, M.-C. Breuil, L.H. Hansen, J.C. Setubal, L. Philippot, Impact of phages on soil bacterial communities and nitrogen availability under different assembly scenarios, Microbiome 8 (2020) 1–14, https://doi.org/10.1186/s40168-020-00822-z.
[16] X. Tang, S. Zhou, Lysogenic phage therapy towards emerging contaminant bioremediation, Sci. China Technol. Sci. 67 (2024) 3129–3131, https://doi.org/10.1007/s11431-024-2728-y.
[17] X. Liu, S. Lu, Y. Liu, Y. Wang, X. Guo, Y. Chen, J. Zhang, F. Wu, Performance and mechanism of sulfamethoxazole removal in different bioelectrochemical technology-integrated constructed wetlands, Water Res. 207 (2021), https://doi.org/10.1016/j.watres.2021.117814.
[18] J. Liang, J. Huang, S. Zhang, X. Yang, S. Huang, L. Zheng, M. Ye, S. Sun, A highly efficient conditioning process to improve sludge dewaterability by combining calcium hypochlorite oxidation, ferric coagulant re-flocculation, and walnut shell skeleton construction, Chem. Eng. J. 361 (2019) 1462–1478, https://doi.org/10.1016/j.cej.2018.10.143.
[19] H. Wang, H. Cui, X. Ma, C.R. Cornell, L. Zhang, Y. Ren, M. Li, Y. Liu, S. Gao, Z. Li, A. Wang, J. Zhou, B. Liang, Molecular mechanism of adsorbing triclocarban by the activated sludge in wastewater treatment systems, Chem. Eng. J. 463 (2023), https://doi.org/10.1016/j.cej.2023.142431.
[20] S. Chen, Y. Zhou, Y. Chen, J. Gu fastp, An ultra-fast all-in-one FASTQ preprocessor, Bioinformatics 34 (2018) 884–890, https://doi.org/10.1093/bioinformatics/bty560.
[21] S. Zhu, Z. Tan, Z. Guo, H. Zheng, B. Zhang, Z. Qin, J. Xie, Y. Lin, B. Sheng, G. Qiu, S. Preis, C. Wei, Symbiotic virus-bacteria interactions in biological treatment of coking wastewater manipulating bacterial physiological activities, Water Res. 257 (2024), https://doi.org/10.1016/j.watres.2024.121741.
[22] D. Hyatt, P.F. LoCascio, L.J. Hauser, E.C. Uberbacher, Gene and translation initiation site prediction in metagenomic sequences, Bioinformatics 28 (2012) 2223–2230, https://doi.org/10.1093/bioinformatics/bts429.
[23] J. Guo, B. Bolduc, A.A. Zayed, A. Varsani, G. Dominguez-Huerta, T.O. Delmont, A.A. Pratama, M.C. Gazitua, D. Vik, M.B. Sullivan, S. Roux, VirSorter2: a multi-classifier, expert-guided approach to detect diverse DNA and RNA viruses, Microbiome 9 (2021), https://doi.org/10.1186/s40168-020-00990-y.
[24] A.P. Camargo, S. Nayfach, I.M.A. Chen, K. Palaniappan, A. Ratner, K. Chu, S.J. Ritter, T.B.K. Reddy, S. Mukherjee, F. Schulz, L. Call, R.Y. Neches, T. Woyke, N.N. Ivanova, E.A. Eloe-Fadrosh, N.C. Kyrpides, S. Roux, IMG/VR v4: an expanded database of uncultivated virus genomes within a framework of extensive functional, taxonomic, and ecological metadata, Nucleic Acids Res. 51 (2023) D733–D743, https://doi.org/10.1093/nar/gkac1037.
[25] J. Shang, Y. Sun, CHERRY: a computational metHod for accuratE pRediction of virus-pRokarYotic interactions using a graph encoder-decoder model, Briefings Bioinf. 23 (2022), https://doi.org/10.1093/bib/bbac182.
[26] Z. Li, D. Pan, G. Wei, W. Pi, C. Zhang, J. Wang, Y. Peng, L. Zhang, Y. Wang, C.R.J. Hubert, X. Dong, Deep sea sediments associated with cold seeps are a subsurface reservoir of viral diversity, ISME J. 15 (2021) 2366–2378, https://doi.org/10.1038/s41396-021-00932-y.
[27] R. Zhao, K. Yu, J. Zhang, G. Zhang, J. Huang, L. Ma, C. Deng, X. Li, B. Li, Deciphering the mobility and bacterial hosts of antibiotic resistance genes under antibiotic selection pressure by metagenomic assembly and binning approaches, Water Res. 186 (2020) 116318, https://doi.org/10.1016/j.watres.2020.116318.
[28] D.H. Huson, S. Mitra, H.-J. Ruscheweyh, N. Weber, S.C. Schuster, Integrative analysis of environmental sequences using MEGAN4, Genome Res. 21 (2011) 1552–1560, https://doi.org/10.1101/gr.120618.111.
[29] J. Liang, J. Liu, P. Jia, T. Yang, Q.-w. Zeng, S. Zhang, B. Liao, W. Shu, J. Li, Novel phosphate-solubilizing bacteria enhance soil phosphorus cycling following ecological restoration of land degraded by mining, ISME J. 14 (2020) 1600–1613, https://doi.org/10.1038/s41396-020-0632-4.
[30] Z. Zhou, P.Q. Tran, A.M. Breister, Y. Liu, K. Kieft, E.S. Cowley, U. Karaoz, K. Anantharaman, METABOLIC: high-throughput profiling of microbial genomes for functional traits, metabolism, biogeochemistry, and community-scale functional networks, Microbiome 10 (2022) 33, https://doi.org/10.1186/s40168-021-01213-8.
[31] D. Piel, M. Bruto, Y. Labreuche, F. Blanquart, D. Goudenege, R. Barcia-Cruz, S. Chenivesse, S. Le Panse, A. James, J. Dubert, B. Petton, E. Lieberman, K.M. Wegner, F.A. Hussain, K.M. Kauffman, M.F. Polz, D. Bikard, S. Gandon, E.P.C. Rocha, F. Le Roux, Phage-host coevolution in natural populations, Nat. Microbiol. 7 (2022) 1075–1086, https://doi.org/10.1038/s41564-022-01157-1.
[32] M. Bastian, S. Heymann, M. Jacomy, Gephi: an open source software for exploring and manipulating networks, Proceed. Int. AAAI Conf. Web. Soc. Med. (2009) 361–362.
[33] D. Huang, R. Xia, C. Chen, J. Liao, L. Chen, D. Wang, P.J. Alvarez, P. Yu, Adaptive strategies and ecological roles of phages in habitats under physicochemical stress, Trends Microbiol. 32 (2024) 902–916, https://doi.org/10.1016/j.tim.2024.02.002.
[34] J. Wang, S. Wang, Microbial degradation of sulfamethoxazole in the environment, Appl. Microbiol. Biotechnol. 102 (2018) 3573–3582, https://doi.org/10.1007/s00253-018-8845-4.
[35] R. Sun, P. Yu, P. Zuo, D. Villagran, J. Mathieu, P.J.J. Alvarez, Biofilm control in flow-through systems using polyvalent phages delivered by peptide-modified M13 coliphages with enhanced polysaccharide affinity, Environ. Sci. Technol. 56 (2022) 17177–17187, https://doi.org/10.1021/acs.est.2c06561.
[36] J.G. McCutcheon, A. Lin, J.J. Dennis, Characterization of Stenotrophomonas maltophilia phage AXL1 as a member of the genus Pamexvirus encoding resistance to trimethoprim-sulfamethoxazole, Sci. Rep. 12 (2022), https://doi.org/10.1038/s41598-022-14025-z.
[37] Y. Zhu, Y. Zhang, S. Yan, X. Chen, S. Xie, Viral community structure and functional potential vary with lifestyle and altitude in soils of mt. Everest, Environ. Int. 178 (2023), https://doi.org/10.1016/j.envint.2023.108055.
[38] R. Cheng, X. Li, L. Jiang, L. Gong, C. Geslin, Z. Shao, Virus diversity and interactions with hosts in deep-sea hydrothermal vents, Microbiome 10 (2022) 235.
[39] O. Kimchi, Y. Meir, N.S. Wingreen, Lytic and temperate phage naturally coexist in a dynamic population model, ISME J. 18 (2024), https://doi.org/10.1093/ismejo/wrae093.
[40] X. Luo, P. Wang, J. Li, M. Ahmad, L. Duan, L. Yin, Q. Deng, B. Fang, S. Li, W. Li, Viral community-wide auxiliary metabolic genes differ by lifestyles, habitats, and hosts, Microbiome 10 (2022) 190, https://doi.org/10.1186/s40168-022-01384-y.
[41] A.E. Zimmerman, C. Howard-Varona, D.M. Needham, S.G. John, A.Z. Worden, M.B. Sullivan, J.R. Waldbauer, M.L. Coleman, Metabolic and biogeochemical consequences of viral infection in aquatic ecosystems, Nat. Rev. Microbiol. 18 (2020) 21–34, https://doi.org/10.1038/s41579-019-0270-x.
[42] M. Qi, B. Liang, L. Zhang, X. Ma, L. Yan, W. Dong, D. Kong, L. Zhang, H. Zhu, S. Gao, J. Jiang, S. Liu, P.F.X. Corvini, A. Wang, Microbial interactions drive the complete catabolism of the antibiotic sulfamethoxazole in activated sludge microbiomes, Environ. Sci. Technol. 55 (2021) 3270–3282, https://doi.org/10.1021/acs.est.0c06687.
[43] S.I. Mulla, A. Hu, Q. Sun, J. Li, F. Suanon, M. Ashfaq, C.-P. Yu, Biodegradation of sulfamethoxazole in bacteria from three different origins, J. Environ. Manag. 206 (2018) 93–102, https://doi.org/10.1016/j.jenvman.2017.10.029.
[44] P.J.M. Reis, A.C. Reis, B. Ricken, B.A. Kolvenbach, C.M. Manaia, P.F.X. Corvini, O.C. Nunes, Biodegradation of sulfamethoxazole and other sulfonamides by Achromobacter denitrificans PR1, J. Hazard Mater. 280 (2014) 741–749, https://doi.org/10.1016/j.jhazmat.2014.08.039.
[45] K. Chen, J. Feng, P.L.E. Bodelier, Z. Yang, Q. Huang, M. Delgado-Baquerizo, P. Cai, W. Tan, Y. Liu, Metabolic coupling between soil aerobic methanotrophs and denitrifiers in rice paddy fields, Nat. Commun. 15 (2024), https://doi.org/10.1038/s41467-024-47827-y.
[46] F. Revesz, M. Farkas, B. Kriszt, S. Szoboszlay, T. Benedek, A. Tancsics, Effect of oxygen limitation on the enrichment of bacteria degrading either benzene or toluene and the identification of Malikia spinosa (Comamonadaceae) as prominent aerobic benzene-, toluene-, and ethylbenzene-degrading bacterium: enrichment, isolation and whole-genome analysis, Environ. Sci. Pollut. Control Ser. 27 (2020) 31130–31142, https://doi.org/10.1007/s11356-020-09277-z.
[47] S. Zhou, D. Yang, Q. Xu, Z. Yang, M. Jin, J. Yin, H. Wang, K. Zhou, L. Wang, J. Li, Z. Shen, Presence of bacteroidales as a predicator of human enteric viruses in Haihe River of Tianjin City, China, Environ. Sci. Pollut. Control Ser. 26 (2019) 8169–8181, https://doi.org/10.1007/s11356-019-04217-y.
[48] M. Yu, M. Zhang, R. Zeng, R. Cheng, R. Zhang, Y. Hou, F. Kuang, X. Feng, X. Dong, Y. Li, Z. Shao, M. Jin, Diversity and potential host-interactions of viruses inhabiting deep-sea seamount sediments, Nat. Commun. 15 (2024), https://doi.org/10.1038/s41467-024-47600-1.
[49] L. Yuan, F. Ju, Potential auxiliary metabolic capabilities and activities reveal biochemical impacts of viruses in municipal wastewater treatment plants, Environ. Sci. Technol. 57 (2023) 5485–5498, https://doi.org/10.1021/acs.est.2c07800.
[50] H.C. Tu, M.Y. Lin, C.Y. Lin, T.H. Hsiao, Z.H. Wen, B.H. Chen, T.F. Fu, Supplementation with 5-formyltetrahydrofolate alleviates ultraviolet B-inflicted oxidative damage in folate-deficient zebrafish, Ecotoxicol. Environ. Saf. 182 (2019), https://doi.org/10.1016/j.ecoenv.2019.109380.
[51] S.W. Wilhelm, C.A.J.B. Suttle, Viruses and nutrient cycles in the sea: viruses play critical roles in the structure and function of aquatic food webs, Bioscience 49 (1999) 781–788, https://doi.org/10.2307/1313569.
[52] Y. Tan, P. Yu, D. Huang, M.M. Yuan, Z. Yu, H. Lu, P.J.J. Alvarez, L. Zhu, Enhanced bacterium-phage symbiosis in attached microbial aggregates on a membrane surface facing elevated hydraulic stress, Environ. Sci. Technol. 57 (2023) 17324–17337, https://doi.org/10.1021/acs.est.3c05452.
[53] K. Kieft, Z. Zhou, R.E. Anderson, A. Buchan, B.J. Campbell, S.J. Hallam, M. Hess, M.B. Sullivan, D.A. Walsh, S. Roux, K. Anantharaman, Ecology of inorganic sulfur auxiliary metabolism in widespread bacteriophages, Nat. Commun. 12 (2021) 3503, https://doi.org/10.1038/s41467-021-23698-5.
[54] M.A. Moran, B.P. Durham, Sulfur metabolites in the pelagic ocean, Nat. Rev. Microbiol. 17 (2019) 665–678, https://doi.org/10.1038/s41579-019-0250-1.
[55] K. Kieft, A.M. Breister, P. Huss, A.M. Linz, E. Zanetakos, Z. Zhou, J. Rahlff, S.P. Esser, A.J. Probst, S. Raman, S. Roux, K. Anantharaman, Virus-associated organosulfur metabolism in human and environmental systems, Cell Rep. 36 (2021) 109471, https://doi.org/10.1016/j.celrep.2021.109471.
[56] X. Shuai, Z. Zhou, X. Ba, Y. Lin, Z. Lin, Z. Liu, X. Yu, J. Zhou, G. Zeng, Z. Ge, H. Chen, Bacteriophages: vectors of or weapons against the transmission of antibiotic resistance genes in hospital wastewater systems? Water Res. 248 (2024) https://doi.org/10.1016/j.watres.2023.120833.
[57] S. Du, L. Bi, D. Lin, X.-Q. Zheng, R. Neilson, D. Zhu, Viral communities suppress the earthworm gut antibiotic resistome by lysing bacteria on a national scale, Environ. Sci. Technol. 58 (2024) 13961–13972, https://doi.org/10.1021/acs.est.4c03812.